An Overview of Coupled Ocean-Atmosphere Models of El Nino and the Southern Oscillation

Julian P. McCREARY, Jr.

Oceanographic Center, Nova University,
8000 North Ocean Drive, Dania, FL 33004 - U.S.A.

1. Introduction

The phenomenon of El Nino and the Southern Oscillation (ENSO) exhibits a time scale of 2-9 years. An intriguing hypothesis, for which there is an increasing body of supportive evidence, is that ENSO is the result of strong coupling between the ocean and the atmosphere in the tropics. A number of coupled models have been developed in the past few years to explore this idea. Specifically, the models address the question: How can the ocean and the atmosphere interact to produce oscillations with the long ENSO time scale?

In this overview, as much as is possible the coupled models discussed are arranged in a hierarchy of increasing dynamical complexity. Useful categories for this purpose are: conceptual models, simple models, intermediate models, and coupled general circulation models (GCM's). **Conceptual models** drastically reduce the spatial structure of the atmosphere and ocean, consisting typically of a few variables and coupled equations that depend only on time, whereas **simple models** represent the ocean and/or atmosphere with simplified, but familiar, sets of partial differential equations. Conceptual and simple models are useful because they illustrate possible fundamental processes of air-sea interaction; they are limited, however, in that it is generally difficult or impossible to compare their solutions closely with observations, and hence many of them are untestable. **Intermediate models** are defined here to be the set of coupled systems that utilize reduced-gravity oceanic and atmospheric models with realistic ocean thermodynamics. They are sophisticated enough to produce realistic solutions and so are testable, and yet they are also simple enough to be relatively easy to diagnose. **Coupled GCM's** can, and should, be closely compared to observations, but the important processes at work in them are not always easy to determine.

2. Conceptual and Simple Models

a. *Oceanic Rossby waves*

McCreary (1983) constructed a simple model which showed how oceanic Rossby waves might be involved in generating the low-frequency oscillations associated with ENSO (Fig. 1). The ocean was a reduced-gravity model [equations (4a)], and sea surface temperature (SST) in the eastern Pacific was specified to be either cold or warm depending on whether the thickness of the upper layer h_e there was less than or greater than a specified thickness h_{cr} (Fig. 1a). The model atmosphere consisted of two patches of zonal wind stress, τ_w and τ_H, that were assumed to interact with the ocean in a way first suggested by Bjerknes (1966, 1969): when the eastern ocean is cool ($h_e < h_{cr}$) the equatorial easterlies τ_w strengthen in the central ocean, thereby simulating Bjerknes' Walker circulation; when the eastern ocean is warm ($h_e > h_{cr}$) the extra-equatorial easterlies τ_H strengthen, thereby simulating an enhanced Hadley circulation. Wind curl associated with τ_H deepens the model interface to form ridge A (panel 1 of Fig. 1b). This ridge subsequently propagates slowly westward as a Rossby wave, and reflects from the western boundary as an equatorially trapped Kelvin wave that gradually deepens h_e (panels 2 and 3). Eventually h_e deepens beyond h_{cr}, SST

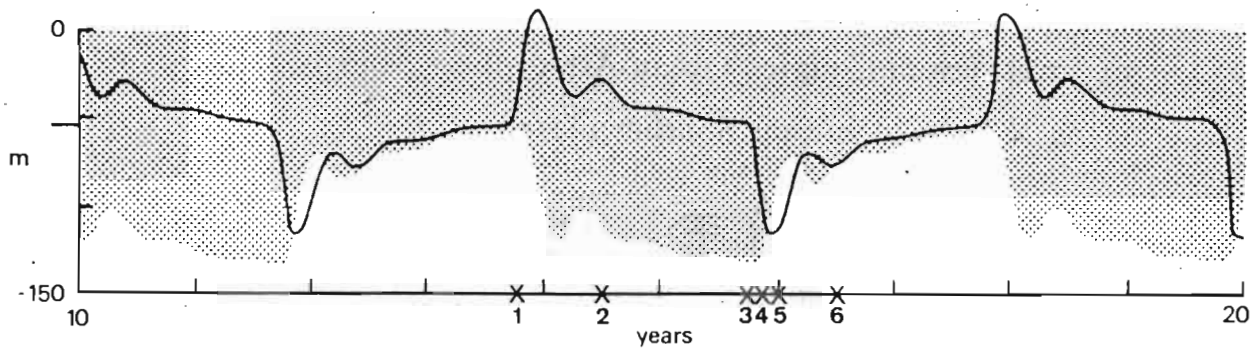

FIG.1a. The thickness of the model interface in the eastern equatorial ocean h_e (solid curve) and in the western equatorial ocean (bottom edge of the shaded area). The straight line indicates the value of h_{cr} = 53.5 m. The x's indicate times of the plots in Figure 1b. Transitions from one wind state to another are marked by El Nino or anti-El Nino events in the eastern ocean. (From McCreary, 1983.)

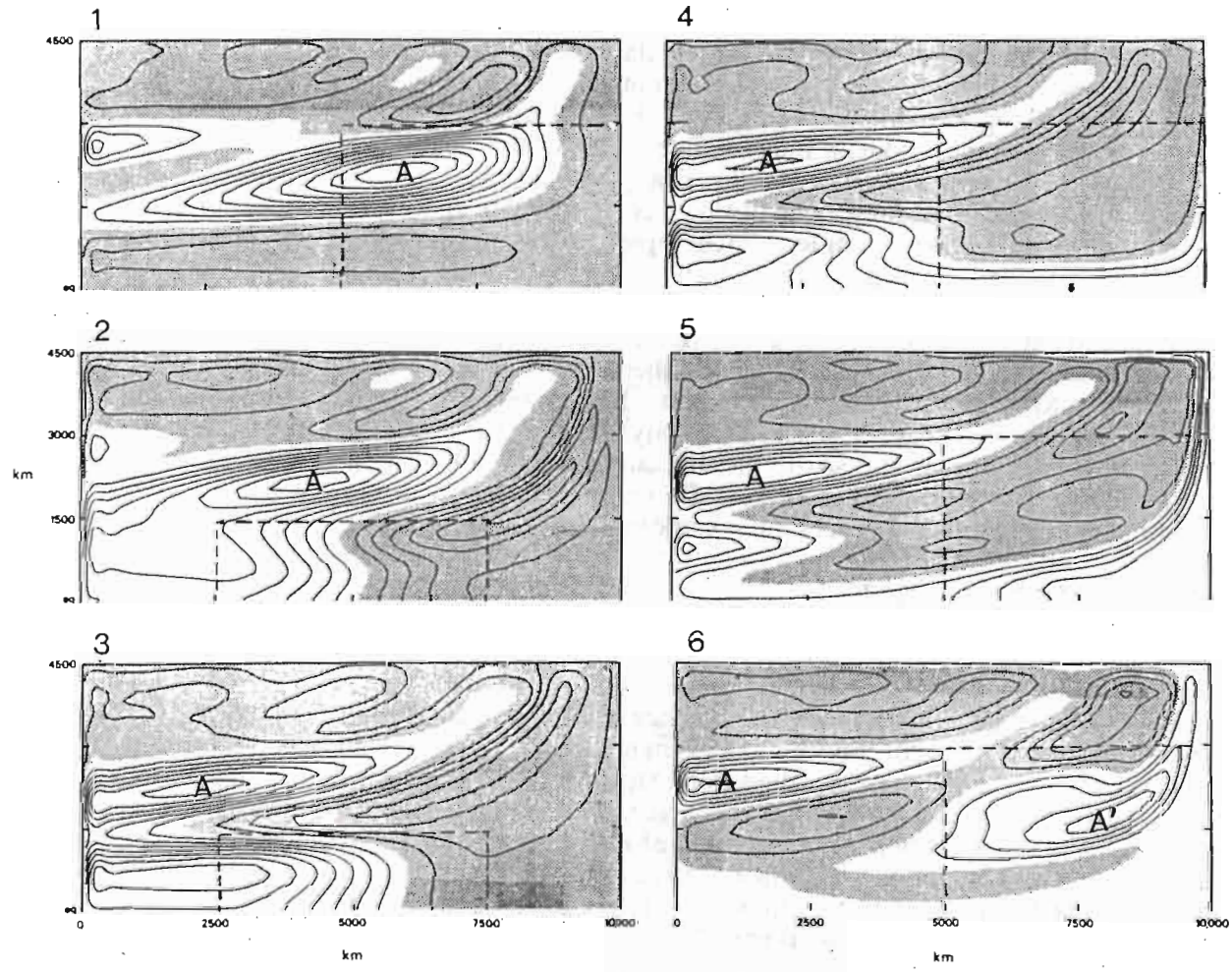

FIG.1b. Plots of upper-layer thickness anomaly for the 6 times indicated in Figure 1a. The contour interval is 10 m, there is no zero contour, and the shaded regions indicate negative anomalies (where h is less than 100 m). The dashed rectangles indicate the location of the wind patches τ_H and τ w. The slow propagation time of ridge A across the ocean basin sets the time scale of the model ENSO. (From McCreary and Anderson, 1984.)

warms in the eastern ocean, and an ENSO event is triggered (panels 4 and 5). It is the long propagation time of ridge A across the ocean basin that sets the period of the oscillation. A new ridge A' begins to spin up that will eventually trigger the next model ENSO at year 20 (panel 6).

Graham and White (1988) presented a conceptual model involving four variables: η_e and T_e representing the anomalies of upper-layer thickness and SST in the eastern Pacific, η_c being the upper-layer thickness anomaly in the off-equatorial central Pacific, and τ denoting the strength of the equatorial zonal wind stress anomaly. The four equations relating these variables are

$$\eta_e(t) = a\, T_e(t) + \eta_c(t-\delta)\,; \qquad \eta_c = -\,c\tau,$$
$$\dot{\tau} = -\,\tau + \alpha\,(ab)^{-1}\, T_e; \qquad Te = b\,\eta_e, \tag{1a}$$

where ε is a stochastic forcing, δ is a time lag, and the dot indicates a time derivative. The relationships in these equations all have sensible physical interpretations. For example, η_e is determined in part by $\eta_c(t-\delta)$, the lag simulating the delayed effect of Rossby waves that reflect from the western ocean boundary (like ridge A in Figure 1b); τ is linearly related to T_e, this relationship modeling Bjerknes' idea that the equatorial winds are determined by SST in the eastern Pacific. Solving for a single equation in τ yields

$$\dot{\tau} = (\alpha-1)\,\tau - c\,\tau\,(t-\delta) + \varepsilon\, d/\alpha \tag{1b}$$

Graham and White (1988) took $\alpha < 1$, so that (1b) is the equation for a damped oscillator. Without external forcing ε, then, the system has no oscillations, but rather adjusts to the state $\tau = 0$. With external forcing but without time-delayed feedback, solutions oscillate at the time scales of ε ; when time delayed feedback is included, they oscillate with a dominant period of the order of δ .

b. *Two equilibrium states*

A limitation of the McCreary (1983) model is that it involves τ_H, a wind component not clearly present in the observations. McCreary and Anderson (1984) modified the earlier model to eliminate τ_H. Parameters of the new system were adjusted so that in the absence of seasonal or random forcing solutions would adjust to one or the other of two equilibrium states: an ENSO state with τ_w switched off, and a "normal" state with τ_w switched on. When a seasonably varying wind stress τ_s is included, solutions can jump from being near one equilibrium state to being near the other (Fig. 2). Note in Figure 2 that after τ_w switches on (for example, after point A) h_e first overshoots and then gradually relaxes back toward its equilibrium depth, a relaxation that is due to Rossby waves reflected from the western boundary. This relaxation must be sufficiently complete before the seasonal cycle can trigger an ENSO event; thus, reflected Rossby waves also play an important role in generating the oscillations in this system. Note also that the onset of the model ENSO is phase located to the warm phase of the annual cycle (h_e deep), consistent with many observed events. With proper adjustment of the critical thickness h_{cr} the solution remains in a normal state longer than an ENSO state (lower panel of Fig. 2).

Schopf (1986) and Suarez and Schopf (1987) discussed solutions to the equation

$$\dot{X}(t) = X(t) - X^3(t) - cX(t-\delta) \tag{2}$$

suggesting that this conceptual model explained the oscillatory behavior of their coupled, numerical model of ENSO (see below). Schopf (1986) also pointed out similarities of this conceptual system to the McCreary and Anderson (1984) model just discussed. Note the

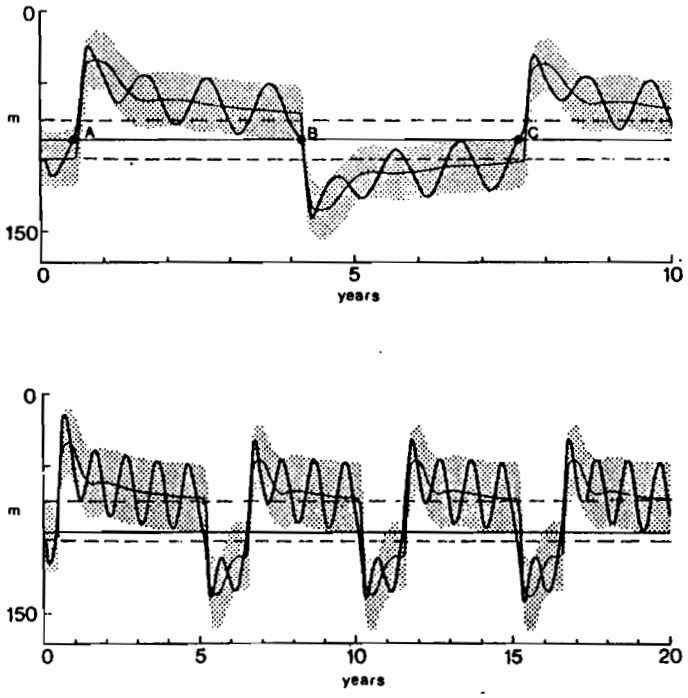

FIG.2. The time development of h_e (solid curves) when h_{cr} = 86.5 m (upper panel) and when h_{cr} = 95.3 m (lower panel). The solid straight lines indicate the values of h_{cr}, and the dashed lines indicate the two equilibrium values of h_e (74 m and 100 m) that are possible when there is no seasonal forcing τ S. In the lower panel, the model remains longer in a "normal" state, and ENSO events last only for 1 - 1 1/2 years. (From McCreary and Anderson, 1984.)

similarity to Graham and White's system (1c), in particular the presence of a time-delayed feedback term. In contrast to (1c), equation (2) has a strong positive feedback term X with a nonlinear negative feedback term $-X^3$ included to limit the growth of unstable perturbations. As a result, without time-delayed feedback the system adjusts to either of the two equilibrium states $X = \pm 1$ (the third equilibrium state $X = 0$ being unstable). With time-delayed feedback, the system develops oscillations at periods greater than 2δ ; indeed, oscillations still occur even if the reflection coefficient c is as small as 0.15.

Vallis (1988) considered a variety of conceptual models. One of them consisted of a one-dimensional equatorial ocean, defined in the domain $0 < x < L$. The system involves three variables: anomalous SST along the equator T(x), an x-independent anomalous zonal wind τ , and an x-independent equatorial zonal current u. The three equations relating these variables are

$$\begin{aligned} T_t + uT_x &= -AT \\ u_t &= \tau + c(u^*-u) + \varepsilon \\ \tau &= B\,[T(L) - T(0)] \end{aligned} \qquad (3)$$

where u^* represents a surface current due to the background trades, and ε is a random forcing. Boundary conditions for the T-equation are: $T(0) = 0$ if $u > 0$ and $T(L) = 0$ if $u < 0$, ensuring that the ocean advects water into the domain that is neither anomalously warm or cold. Again the physical processes described by (3) are sensible; for example, the last of equations (3) expresses Bjerknes' idea that the equatorial wind τ is determined by the SST difference between the eastern and western Pacific Ocean. Without stochastic forcing, the system adjusts to either a normal state with $u < 0$ and a cool eastern ocean, or an El Nino state with $u > 0$ and a warm eastern ocean. Figure 3 shows time series that result for various choices of model parameters. For sufficiently strong stochastic forcing and with $u^* < 0$, the system usually remains near the normal state, but occasionally jumps to being near the El Nino State (panel d of Fig. 3). It is not clear just what sets the time scale for ENSO events in panel d; the system lacks time-delayed feedback, and so the time scale is probably due to the particular nature of the stochastic forcing.

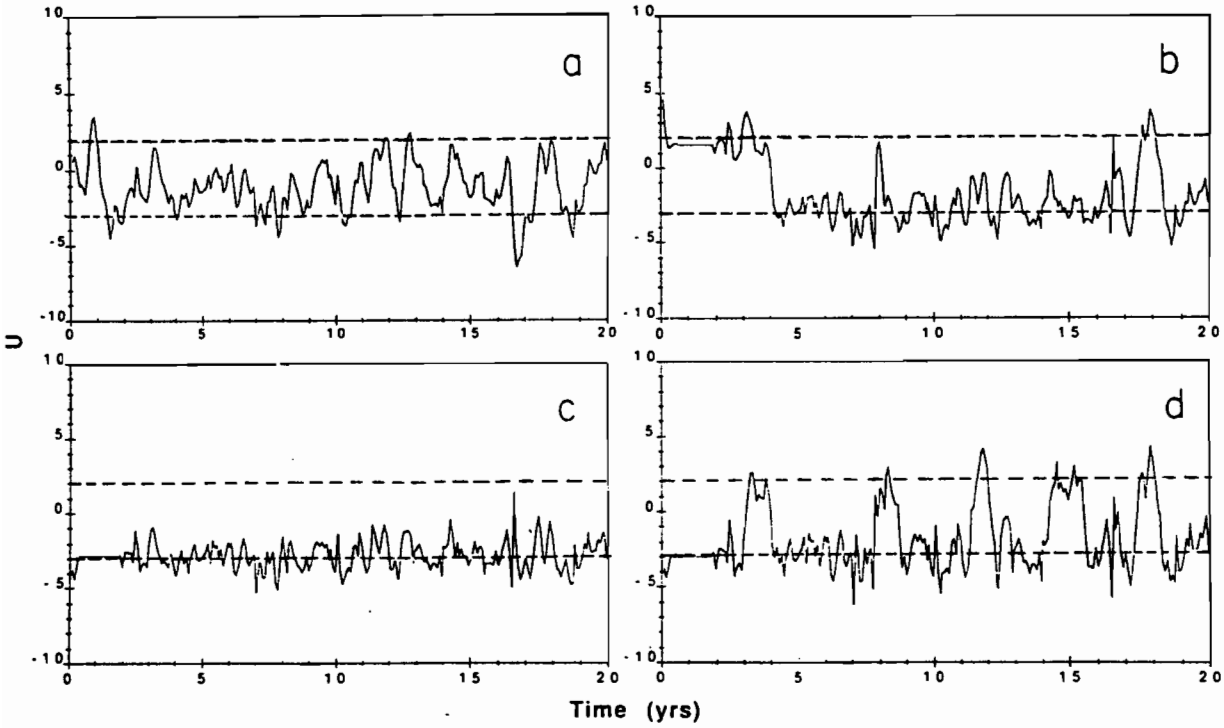

FIG.3. Time series of zonal current u, showing effects of variations of parameters. The dashed lines show the two equilibrium states to which the model will adjust in the absence of random forcing ε. Panel (a): B = 0, so that there is no temperature feedback. Panel (b): As for panel (a), but with $B \neq 0$. Panel (c): As for panel (b), but ε has a shorter correlation time scale. Panel (d): As for panel (c), except that ε has a larger amplitude. (From Vallis, 1988.)

c. *Unstable coupled modes*

Coupled models that study unstable modes nearly all utilize linear, reduced-gravity models of both the ocean and the atmosphere. Equations of motion for the model ocean are

$$u_t - fv + g' \eta_x = -\upsilon u + \tau^x/d,$$

$$v_t + fu + g'\eta_y = -\upsilon v + \tau^y/d, \qquad (4a)$$

$$\eta_t + d\,(u_x + \upsilon_y) = 0,$$

where d is the undisturbed thickness of the upper layer, and a simple equation like

$$T = \sigma \eta \qquad (4b)$$

describes ocean thermodynamics. Equation (4b) states that the anomalous temperature of the upper layer is directly proportional to the anomalous thickness of the upper layer, a relation that models the effect of equatorial upwelling on SST; Hirst (1985, 1986) has also modified (4b) to include a term representing the zonal advection of SST (see below). Equations for the model atmosphere are:

$$U_t - fV + g'' H_x = -AU$$

$$V_t + fU + g'' H_y = - AV \qquad (4c)$$
$$H_t + D (U_x + V_y) = - BH + Q.$$

Typically, the time derivative terms are ignored in (4c), a valid assumption because the atmosphere rapidly adjusts to equilibrium with the slowly varying forcing Q; an exception occurs when equations (4c) include effects of moisture convergence (see the discussion at the end of this section). Coupling between the two systems is provided by

$$\tau^x/d = \gamma U; \quad \tau^y/d = \gamma V; \quad Q = - \alpha T/\sigma \qquad (4d)$$

Solutions to equations (4) are found either numerically or by looking for mode solutions proportional to exp(ikx - iω t), in which case the operators ∂_x and ∂_t are replaced by the imaginary numbers ik and -iω , respectively.

Lau (1981) considered a simpler version of system (4) in order to understand the coupling that might exist between oceanic and atmospheric Kelvin waves. Essentially, he dropped f, v, V and τ^y from (4) and neglected y-derivatives. Mode solutions to this system satisfy the quadratic dispersion relation

$$(\omega^2 - c^2_a k^2) (\omega^2 - c^2_0 k^2) = \omega^2_c \; k^2 c^2_o \qquad (5a)$$

where $c_a = (g'D)^{1/2}$ and $c_o = (g'd)^{1/2}$ are the phase speeds of atmospheric and oceanic Kelvin waves, respectively, and $\omega_c = \alpha\gamma$ is a parameter measuring the strength of the coupling between the two fluids. Because $c_a >> c_o$, the two solutions to (5a) are approximately

$$c_1 = c_a; \qquad c_2 = c_o (1 - \omega_c^2/k^2c^2_a)^{1/2} \qquad (5b)$$

According to (5b), the phase speed of the atmospheric Kelvin wave c_1 is not much affected by the coupling ω_c, but the speed of the oceanic Kelvin wave c_2 is. As $\omega_c^2/(k^2c_a^2) \cong \phi$ increases to 1, c_2 decreases to zero, and for larger values it is imaginary; thus, for $\phi > 1$ this coupled mode is unstable.

The unstable solution in (5b) describes a fundamental process of air-sea interaction that appears to occur in most of the more complex models of ENSO. Figure 4 illustrates that process schematically. Suppose initially that the interface deepens by an amount η . This deepening causes an increase in T [equation (4b)], an increase in Q [equation (4d)], a convergent wind field U [the third of equations (4c)], and convergent ocean currents u [equations (4a)]; the convergent u-field leads to a further increase in η, and so on.

Hirst (1985, 1986) and Yamagata (1985) looked for mode solutions to the full system (4), and their resulting dispersion relations are shown in Figure 5. In each case there is a root with $\omega_i > 0$, a growing instability. This solution also propagates eastward with a phase speed (ω_r/k) similar to, but slower than, the oceanic Kelvin wave speed. Indeed for weaker coupling this root reduces to that of an ordinary oceanic Kelvin wave, leading both Hirst and Yamagata to refer to this unstable root as a "coupled Kelvin wave"; in order to differentiate more clearly this root from its uncoupled counterpart, I will subsequently refer to it as the "Kelvin mode". The process causing the instability is essentially that shown schematically in Figure 4. The upper panel of Figure 8b shows the horizontal structure of Hirst's Kelvin mode; note its similarity along the equator to the diagram in Figure 4, the primary difference being that the region of convergent winds and currents is shifted somewhat east of the maximum of η .

Figure 5 also has dispersion curves of several decaying Rossby modes. Hirst considered an alternate form of ocean thermodynamics in which (4b) was replaced by:
$T_t + u \langle T_x \rangle = 0$, where $\langle T_x \rangle$ is an assumed background temperature gradient. With this

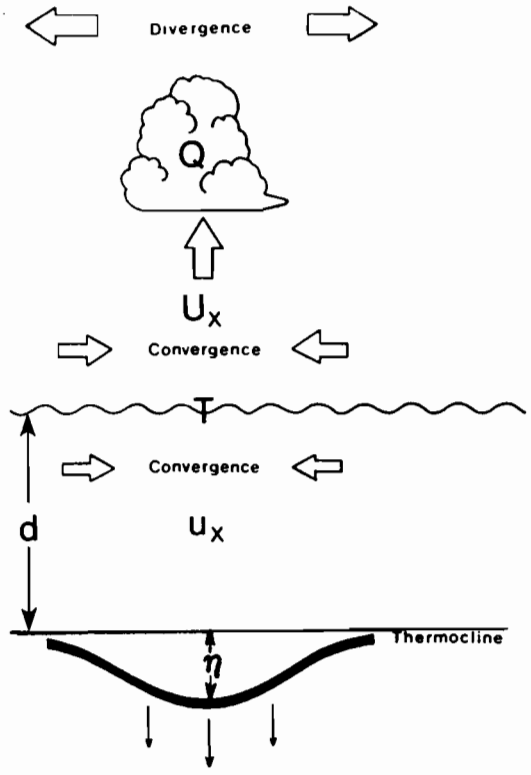

FIG.4. A schematic picture illustrating an important mechanism of unstable air-sea interaction in the tropics. An anomalous increase in the thickness of the upper layer η leads to a positive SST anomaly T, strenghtened atmospheric heating Q, a convergent wind field U_x, and a convergent oceanic flow u_x, which can further increase η. (From Yamagata, 1985.)

ocean thermodynamics, the system has growing Rossby modes and decaying Kelvin modes. It is not clear whether growing Rossby modes play an important role in more complex models, although Philander et al. (1989) suggest that they might exist in their coupled model (see section 4).

Philander et al. (1984) solved equations (4) numerically without using the normal-mode approach. Figure 6 shows the response of their model to an initial increase of interface depth. A growing disturbance develops that propagates eastward at a speed of about 43 $cm.s^{-1}$ considerably slower than that of an uncoupled oceanic Kelvin wave. Hirst (1986) concluded that the instability in Figure 6 was due to the presence of unstable Kelvin modes (upper panel of Fig. 8b).

A problem with all the preceding models of unstable modes is that their solutions continue to grow indefinitely. Anderson and McCreary (1985a) considered a coupled system similar to equations (4), in which the ocean thermodynamics was improved to ensure that T had a realistic upper bound. Consequently, the heating of the atmosphere Q was also bounded, and unstable modes were limited in amplitude. Figure 7 shows the equatorial T field that results when both the ocean and atmosphere are assumed to be cyclic with a wavelength of 15,000 km. After a spin-up period of about 1 year an instability appears that rapidly grows to attain an equilibrium amplitude. It has a period of 2000 days and a very slow eastward propagation speed of 15,000/2,000 $km.day^{-1}$ = 8.7 $cm.s^{-1}$. Anderson and McCreary argued that the mechanism generating this instability is the same as that illustrated in Figure 4. Thus, the instability appears to be a very slowly propagating Kelvin mode, its slow propagation speed probably being due to the fact that the mode is no longer growing in amplitude.

Hirst (1988) extended his earlier mode calculations to include ocean boundaries. Figure 8a shows the SST anomaly that develops when the atmosphere is cyclic with a wavelength of 30,000 km but the ocean is bounded with a width of 15,000 km. Anomalies appear in the western ocean, propagate eastward with a speed of 32 $cm.s^{-1}$, and intensify. When they

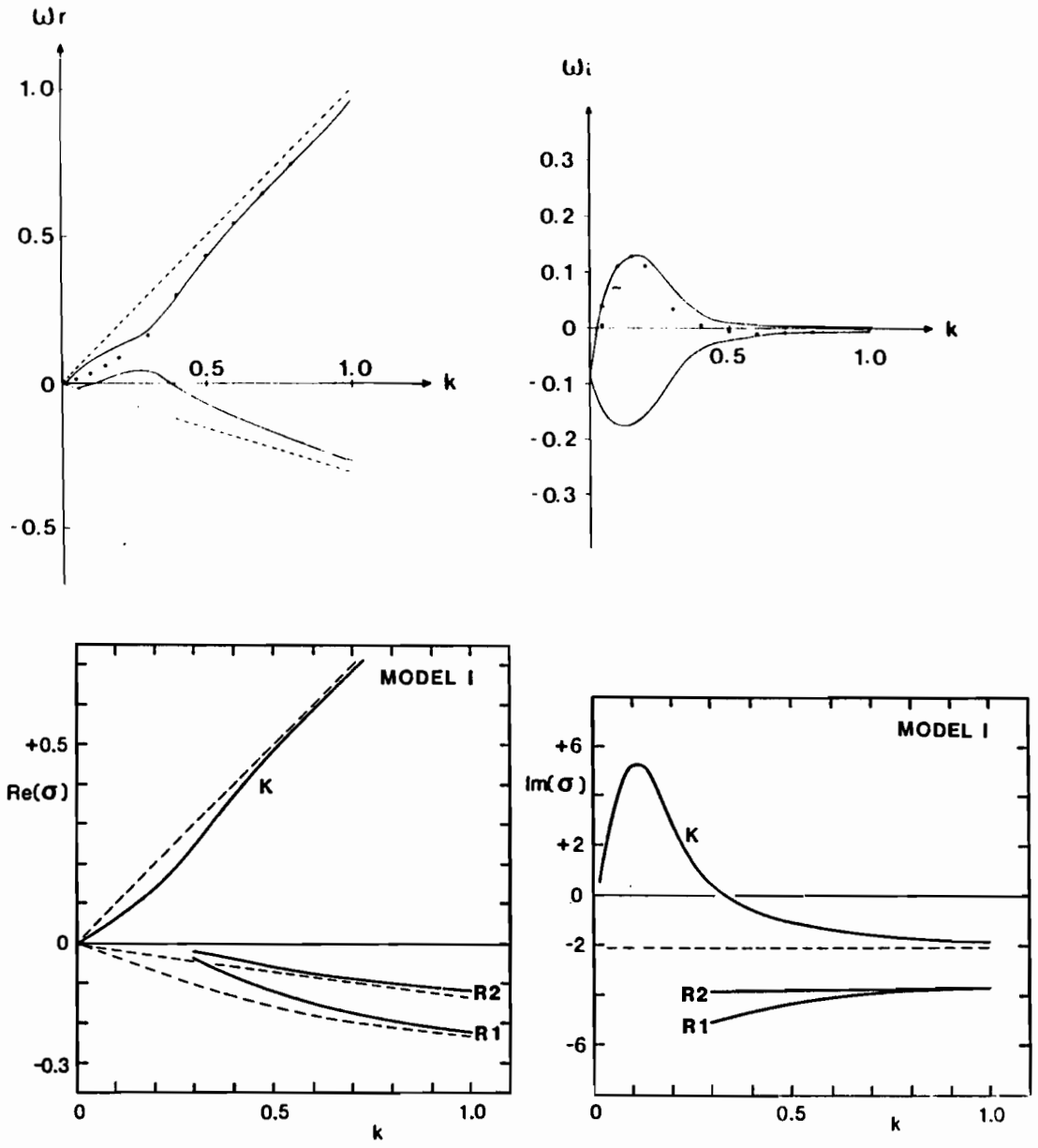

FIG.5. Dispersion curves for the coupled-mode solutions to equations (4) from Yamagata (1985) and Hirst (1986), in the upper and lower panels, respectively. The ω and k axes are normalized using the usual equatorial ocean length and times scales, and both the real and imaginary parts of ω are plotted. Dashed lines in the left panels are the dispersion curves of oceanic Kelvin and Rossby waves in the absence of coupling.

reach the eastern boundary they weaken, and eventually vanish. Figure 8b contrasts the solutions in the bounded ocean (lower panel) with the Kelvin-mode instability in an unbounded ocean (upper panel). The striking property is the similarity in the structure and propagation speed of the two solutions. Hirst concluded that the Kelvin-mode instability was crucial to the dynamics of the oscillation in the bounded, as well as unbounded, ocean.

Finally, it is worth noting that Lau and Shen (1988) and Hirst and Lau (1989) found mode solutions to the coupled system (4) when the atmospheric Kelvin-wave speed c_a was greatly reduced from its dry value by including a term in (4c) parameterizating low-level

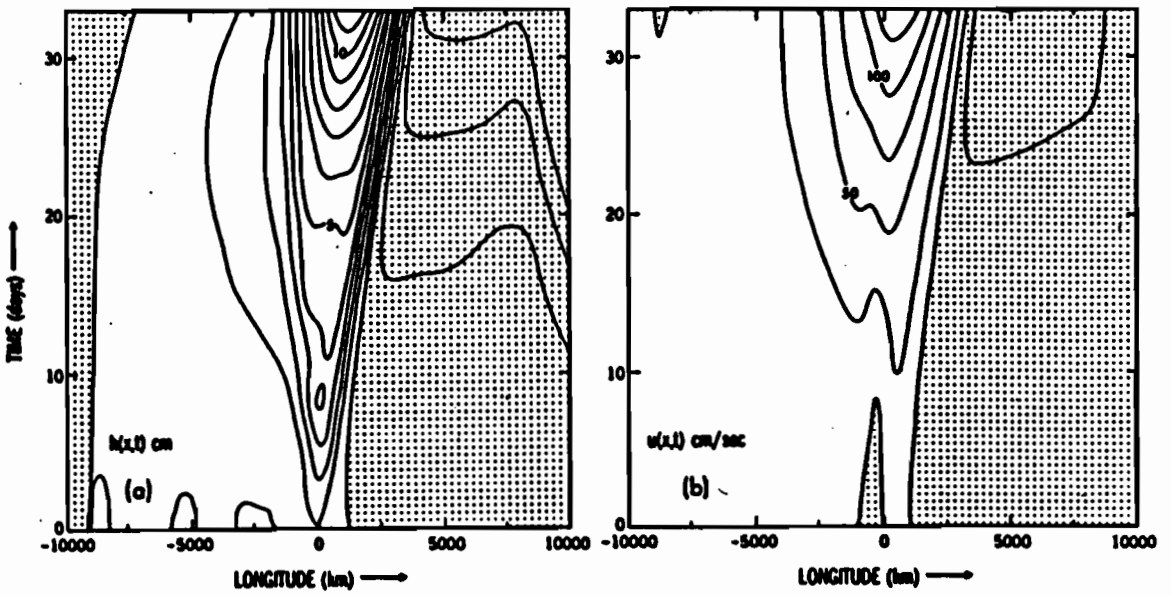

FIG.6. Upper-layer thickness anomaly (left panel) and zonal oceanic current (right panel) in a numerical solution of equations (4), in which an initial positive anomaly of upper-layer thickness is imposed. An instability develops that propagates eastward with a speed of about 43 cm.s^{-1}, considerably slower than that of an uncoupled oceanic Kelvin wave. Compare this instability with the unstable Kelvin mode in the upper panel of Figure 8b. (From Philander et al., 1984.)

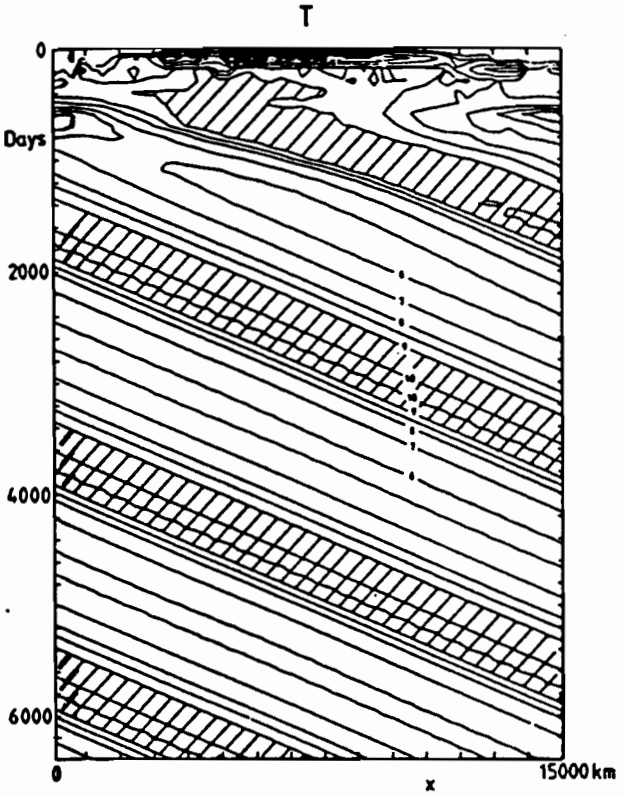

FIG.7. A longitude-time plot of equatorial temperature in a coupled model with cyclic boundary conditions and more realistic ocean thermodynamics. SST relative to a deep ocean temperature of 20^{o}C is shown. After an initial spin-up period, a coupled instability develops that propagates very slowly eastward with a speed of only 8.7 cm.s^{-1}. The improved ocean thermodynamics prevents SST from increasing much beyond 30^{o}C, and so the instability reaches an equilibrium amplitude. (From Anderson and McCreary, 1985.)

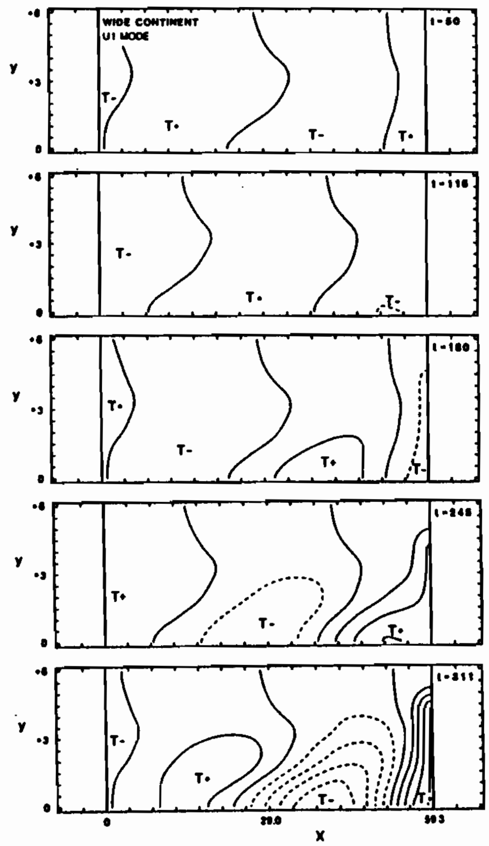

FIG.8a. Plots of SST anomaly for an unstable mode calculation in a bounded ocean basin. Values of x,y and t are in non-dimension units with one unit of space being 2.3° and of time being 2.1 days; thus, the width of the basin is 15,000 km, and the period of the oscillation is 548 days. (From Hirst, 1988.)

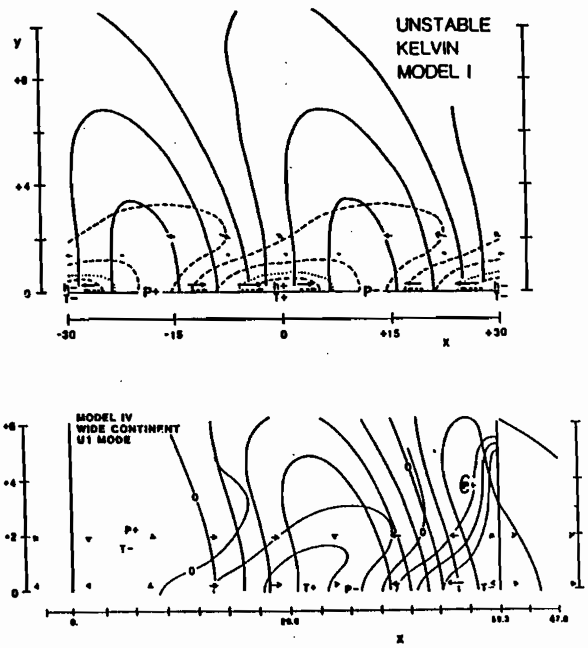

FIG.8b. As in Figure 8a, except showing plots of SST anomaly T (dashed lines or thin solid lines), atmospheric pressure P (thick solid lines), and wind (arrows) for an unstable mode calculation when the ocean is unbounded (upper panel) and bounded (lower panel). The similarity in structure and propagation speed of the two solutions identifies the unstable mode in the lower panel (and in Fig. 8a) as being the unstable Kelvin mode. (From Hirst, 1986, 1988.)

moisture convergence. In this case, the atmosphere no longer adjusts rapidly with respect to the ocean, and so it is necessary to retain the time-derivative terms in equations (4c). Low-frequency unstable waves, similar to those in Figure 5, still exist. In addition, when $c_a \sim c_o$ there is a new set of high-frequency waves with periods of 30-70 days that are essentially coupled oceanic and atmospheric Kelvin waves. The authors hypothesized that the presence of these high-frequency modes help to trigger ENSO events.

3. Intermediate models

Anderson and McCreary (1985a, 1985b) also reported several solutions when the atmosphere was cyclic with a wavelength of 30,000 km but the ocean was bounded. Figure 9a shows the resulting equatorial T when the ocean basin is confined to the region 15,000 < x < 30,000 km and there is an external, atmospheric heating function Q_l imposed over land to the west of the ocean representing the heating associated with convection over Indonesia. The system develops an oscillation with a period of about 4.5 years. Similar to the mode solution in Figure 8a, instabilities appear in the western or central ocean, propagate slowly eastward with a speed of roughly 15,000/1,600 km.day^{-1} = 11 cm.s^{-1}, and eventually dissipate near the eastern boundary. The dissipation is clearly associated with the growth of

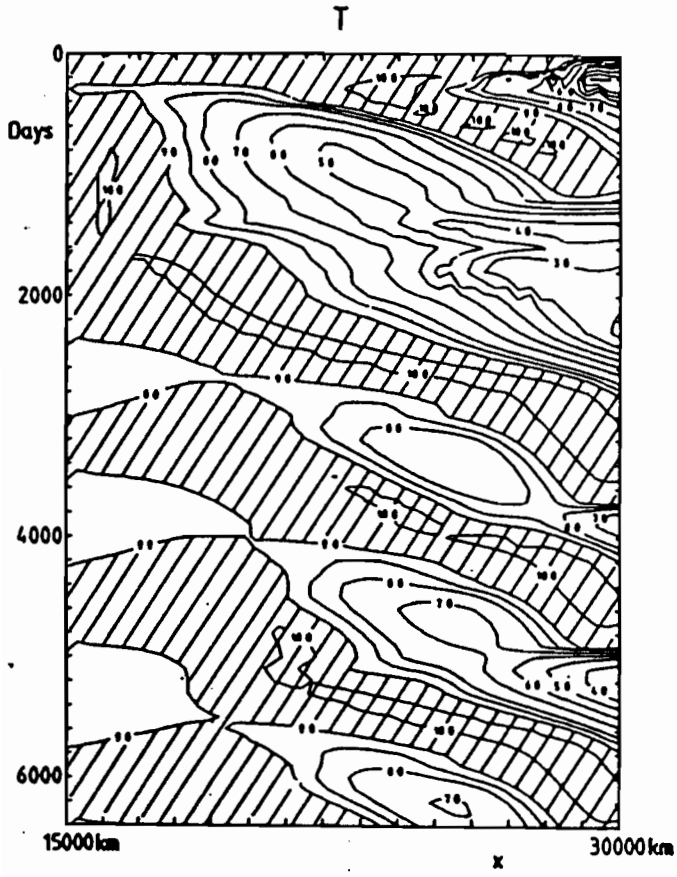

FIG.9a. As in Figure 7, except in a bounded ocean basin. The system develops an oscillation with a period of about 4.5 years. (From McCreary and Anderson, 1985a).

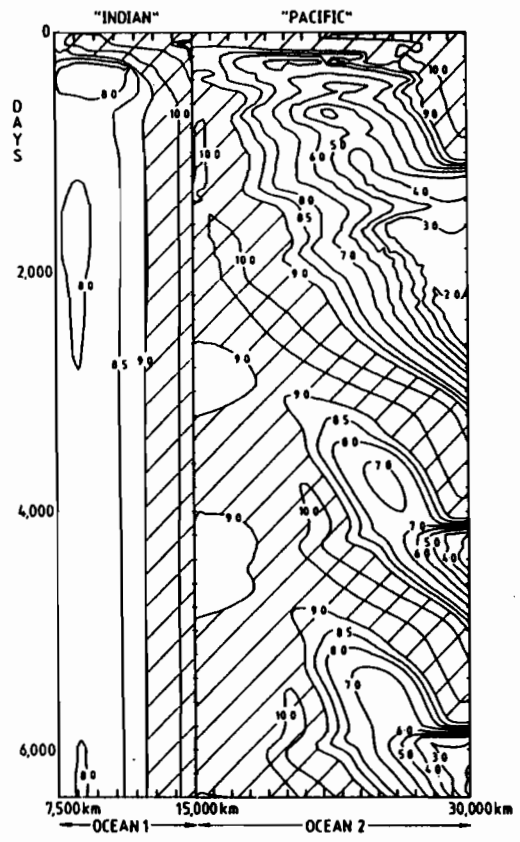

FIG.9b. As in Fig. 9a, except that an "Indian Ocean" is included. The "Indian Ocean" adjusts to an equilibrium state with warmest water in the east, whereas the "Pacific Ocean" undergoes low-frequency oscillations very similar to those in Figure 9a. (From McCreary and Anderson, 1985b.)

another disturbance in the west. Anderson and McCreary, noting the similarity between Figures 7 and 9a, concluded that an important part of the dynamics of the oscillation was the generation of a Kelvin-mode type of instability; they did not comment on whether reflected Rossby waves might also be involved. Hirst (1986) also remarked that a Kelvin-mode instability must account for the oscillation in Figure 9a, suggesting that its slow propagation speed was due to the use of large coupling coefficients. As noted earlier, the slow speed may also be due to the fact that the solution in Figure 9a is not a growing mode, but rather is adjusted to an equilibrium amplitude.

As might be expected, the strength of Q_1 in the preceding model strongly influences the response: with $Q_1 = 0$, an equilibrium state is reached with SST warmest in the eastern ocean (ENSO state), whereas with Q_1 sufficiently large the system adjusts to an equilibrium state with cool eastern SST (a normal state). Budin and Davey (1989) report similar sensitivities to the strength of land convection in their coupled model.

Figure 9b shows a solution to the Anderson and McCreary model when there is a second ocean confined to the region $7500 < x < 15{,}000$ km separated from the first by a thin

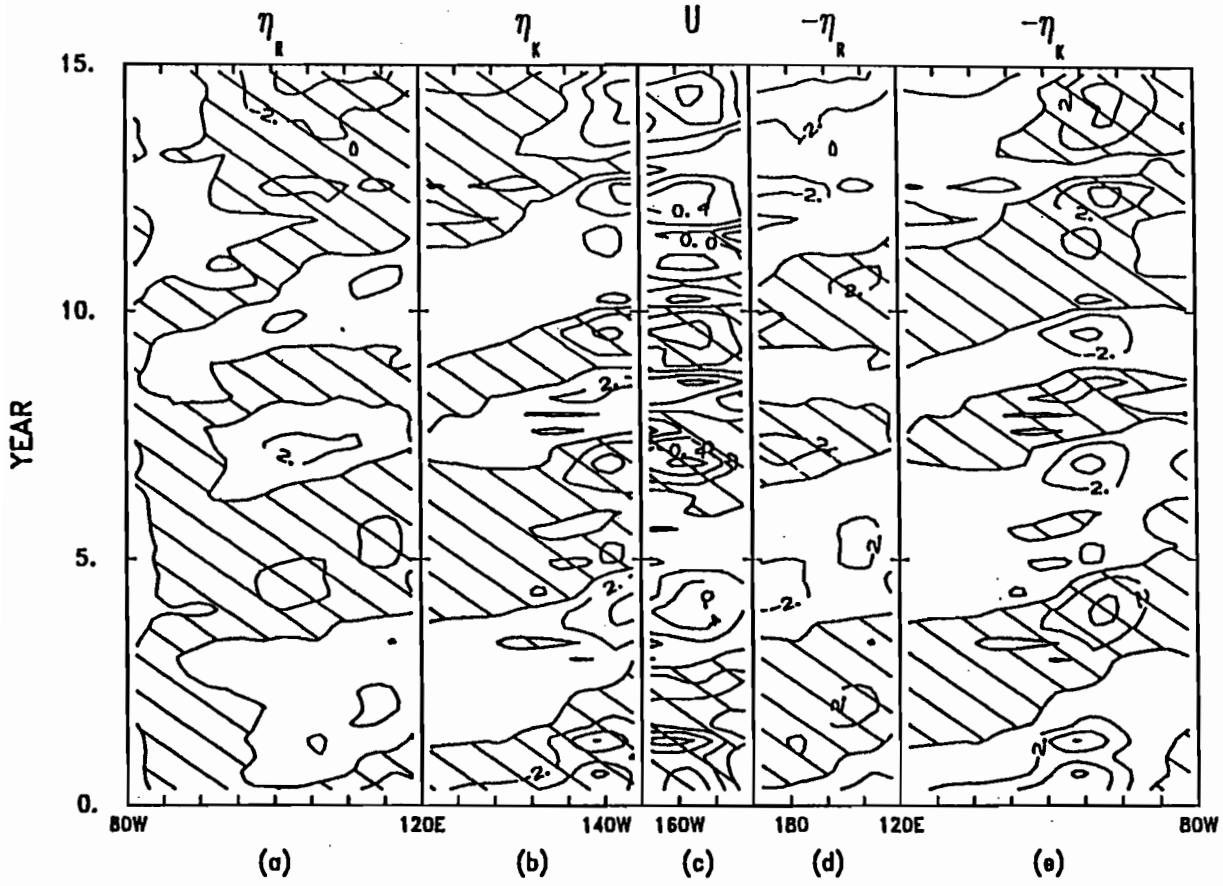

FIG.10. Longitude-time plots of upper-layer-thickness anomalies on the equator η_K and off the equator η_R (averaged from 5°N to 7°N) and of zonal wind U. To illustrate more clearly the importance of westward-propagating Rossby waves, η_R is plotted in reverse from east to west; in addition, in panels (a) - (c) positive anomalies are hatched, whereas in panels (d) and (e) negative anomalies are hatched. The presence of bands sloping upward from left to right suggests the importance of Rossby waves in both the onset and termination of ENSO events.

barrier, and there is no externally imposed forcing Q_1. The smaller "Indian Ocean" quickly adjusts to a stable state with warmest water and strongest atmospheric convection located in the eastern Indian Ocean. The larger "Pacific Ocean" exhibits low-frequency, eastward propagating oscillations, very similar to those in Figure 9a. The similarity of the two solutions in Figure 9 indicates that the model response over the Indian Ocean is dynamically equivalent to specifying Q_1 there.

Schopf and Suarez (1988) developed a coupled ocean-atmosphere model using a 2 1/2 -layer ocean model (a 3-layer model with an inert lower layer) and a 2-layer atmospheric GCM. Figure 10 is a plot showing upper-layer thickness anomaly off the equator (averaged from 5°N to 7°N) η_R and along the equator η_K, and also the zonal wind speed anomaly in the central Pacific U. The solution has an irregular oscillation at ENSO time scales. The irregularity is traceable to the generation of atmospheric variability by nonlinearities associated with the GCM; in a solution utilizing a linearized version of the GCM, the oscillations were perfectly periodic. In Figure 10, η_R is plotted in reverse (from east to west) in order to illustrate the important effect of the propagation of Rossby waves. About year 2, for example, a positive anomaly in η_R appears in the western Pacific and propagates westward as a Rossby wave; the Rossby wave reflects from the western boundary and

increases η_K; this increase triggers the development of a Kelvin-mode instability that increases U (weakens the equatorial wind), and causes an ENSO event about year 4. The positive wind anomaly at this time also acts to raise η R in the western ocean, generating a negative-anomaly Rossby wave that eventually triggers the end of the ENSO event. Interestingly, this sequence of events is very similar to that in the simple model of Figure 1, with the atmospheric switch from τ w to τ_H in the simpler model being replaced here by the development of a Kelvin-mode instability.

The Zebiak and Cane (1987) model is a coupled system similar to (4) except for the following differences: the ocean model has an embedded mixed layer and realistic ocean thermodynamics, climatological winds are included as an external forcing in order to maintain a realistic background ocean circulation, and a parameterization of moisture convergence is added to the specification of Q. Solutions oscillate at ENSO time scales, and are somewhat irregular due to the moisture-convergence term. Battisti (1988) used their model, and diagnosed its response for the presence of Rossby waves and Kelvin waves (modes). He concluded that the dynamics of the oscillations were much the same as in the Schopf and Suarez (1988) model. In particular, reflected Rossby waves were involved in both the onset and decay of ENSO; indeed, in a run in which the reflection of Rossby waves was suppressed, the coupled system adjusted to a permanent ENSO state.

4. Coupled GCM's

At the present, time there are only a few ENSO models that use both oceanic and atmospheric GCM's (a deficiency that no doubt will soon be alleviated). The development of coupled GCM's that can accurately simulate ENSO events is likely to be difficult. Gordon (1989), for example, reports that his solutions tend to adjust toward a permanent ENSO state, and that they are sensitive to the specification of the heat fluxes across the air-sea interface.

The coupled model of Philander et al. (1989) generates low-frequency oscillations. Figure 11a shows time series of eastern Pacific SST anomalies for two cases: when the oceanic GCM has a coarse resolution (4.5° of latitude) and when its resolution is fine (1/3° of latitude near the equator). The low-frequency oscillations in the coarse-resolution model (solid line) propagate westward, and so do not at all resemble ENSO signals; the authors attribute this failure to the fact that the coarse grid cannot resolve the Kelvin-mode instability, and suggest that the westward-propagating disturbances might be related to Hirst's unstable Rossby modes. In contrast, ENSO events in the fine-resolution model develop more realistically via eastward-propagating instabilities. Note in Figure 11b that the weak ENSO event in year 8 appears to be triggered by the reflection of equatorial Rossby waves from the western boundary; compare this time sequence with that of the much simpler model in Figure 1b. On the other hand, there is no obvious reflection of Rossby waves preceding the strong event in year 13. The authors suggest that the onset of ENSO events in their model may be triggered in several different ways.

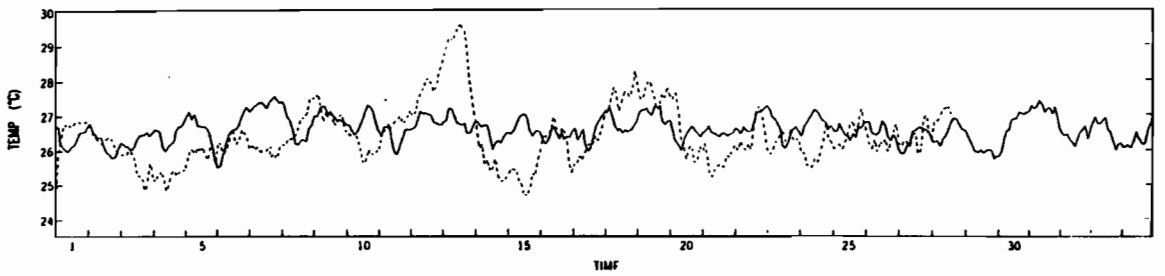

FIG.11a. SST anomalies in the eastern equatorial Pacific Ocean when the coupled model utilizes a coarse-resolution oceanic GCM (solid line) and a fine-resolution oceanic GCM model (dashed line). (From Philander et al. 1989.)

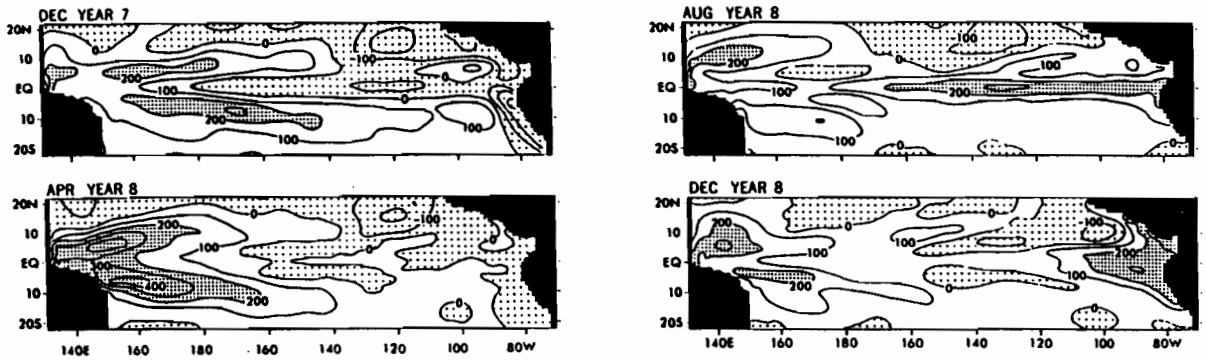

FIG.11b. Vertically integrated temperature from the surface to 300 m in the high-resolution case, effectively showing changes in the depth of the thermocline. The contour interval is 100 cal.cm^{-2}. Lightly stippled regions indicate where the thermocline is elevated, and heavily stippled areas indicate where the thermocline deepening is greater than 200 cal.cm^{-2}. Compare this sequence of panels with those in Figure 1b. (From Philander et al. 1989)

5. Summary and Discussion

Conceptual and simple models illustrate three types of possible ocean-atmosphere interactions that may be involved in ENSO dynamics. In the first type, it is the slow propagation speed of *oceanic Rossby waves* across the basin that sets the oscillation period for ENSO events. In the second, the coupled system has *two equilibrium states* for the same values of model parameters, and a "trigger" causes the system to jump from being near one equilibrium state to being near the other. In the third, slowly propagating *coupled instabilities* develop.

In all of the more complex models, the presence of coupled instabilities, particularly the Kelvin mode, is crucial. In most of them, Rossby waves reflected from the western ocean boundary are involved in both the onset and decay of ENSO; exceptions are the solutions of Philander et al. (1989), and possibly of Anderson and McCreary (1985a, 1985b) who did not discuss the role of Rossby waves in their oscillatory solutions. None of the complex models have been demonstrated to have two equilibrium states, although Suarez and Schopf regard the idea as being useful for discussing the behavior of their system [equation (2)].

Solutions are sensitive to nonlinearities in the model atmosphere: with linearized atmospheres oscillations are exactly periodic, whereas with nonlinear atmospheres they are irregular. They are also sensitive to the specification of convection over Indonesia and the Indian Ocean, and to the parameterization of heat fluxes through the air-sea interface. Clearly, these processes must be properly represented in order to improve models of ENSO.

REFERENCES

Anderson, D.L.T. and J.P. McCreary, 1985a: Slowly propagating disturbances in a coupled ocean-atmosphere model. *J. Atmos. Sci.*, **42**, 615-629.

Anderson, D.L.T. and J.P. McCreary, 1985b: On the role of the Indian Ocean in a coupled ocean-atmosphere model of El Nino and the Southern Oscillation, *J. Atmos. Sci.*, **42**, 2439-2442.

Battisti, D.S., 1988: The dynamics and thermodynamics of a warming event in a coupled tropical atmosphere/ocean model, *J. Atmos. Sci.*, **45**, 2889-2919.

Bjerknes, J., 1966: A possible response of the atmospheric Hadley circulation to equatorial anomalies of ocean temperature. *Tellus*, **18**, 820-829.

Bjerknes, J., 1969: Atmospheric teleconnections from the equatorial Pacific. *Mon. Wea. Rev.*, 163-172.

Budin, G.R. and M.K. Davey, 1989: Land effects in a simple model of the tropical coupled ocean-atmosphere. *Tropical ocean-atmosphere newsletter*, **50**. (Unpublished manuscript.)

Gordon, C., Tropical ocean-atmosphere interactions in a coupled model. (Unpublished manuscript.)

Graham, N.E. and W.B. White, 1988: The El Nino cycle : A natural oscillator of the Pacific ocean-atmosphere. *Science*, **240**, 1293-1302.

Hirst, A.C. 1985: Free equatorial instabilities in simple coupled atmosphere-ocean models. In: *Coupled Ocean-Atmosphere Models*, J.C.J. Nihoul, ed., Elsevier: Amsterdam, 153-165.

Hirst, A.C., 1986: Unstable and damped equatorial modes in simple coupled ocean-atmosphere models. *J. Atmos. Sci.*, **43**, 606-630.

Hirst, A.C., 1988: Slow instabilities in tropical ocean basin-global atmosphere models. *J. Atmos. Sci.*, **45**, 830-852.

Hirst, A.C. and K.-M. Lau, 1989: Intraseasonal and intra-annual oscillations in coupled ocean-atmosphere models. *J. Atmos. Sci.* (In press.)

Lau, K.-M., 1981: Oscillations in a simple equatorial climate system. *J. Atmos. Sci.*, **38**, 248-261.

Lau, K.-M. and Shen, 1988: On the dynamics of intraseasonal oscillations and ENSO. *J. Atmos. Sci.*, **45**, 1781-1797.

McCreary, J.P., 1983: A model of tropical ocean-atmosphere interaction. *Mon. Wea. Rev.*, **111**, 370-387.

McCreary, J.P. and D.L.T. Anderson, 1984: A simple model of El Nino and the Southern Oscillation. *Mon. Wea. Rev.*, **112**, 934-946.

Philander, S.G.H., T. Yamagata and R.C. Pacanowski, 1984: Unstable air-sea interactions in the topics. *J. Atmos. Sci.*, **41**, 604-613.

Philander, S.G.H., N.C. Lau, R.C. Pacanowski, and M.J. Nath, 1989: Two different simulations of the Southern Oscillation and El Nino with coupled ocean-atmosphere general circulation models, *Phil. Trans. Roy. Soc.* (Submitted.)

Schopf, P.S., 1986: Coupled dynamics of the tropical ocean-atmosphere system. In: *Further Progress in Equatorial Oceanography*, E.J. Katz and J. Witte, eds., Nova University Press: Ft. Lauderdale, 279-286.

Schopf, P.S. and M.J. Suarez, 1988: Vacillations in a couple ocean-atmosphere model. *J. Atmos. Sci.*, **45**, 549-566.

Suarez, M.J. and P.S. Schopf, 1988: A delayed action oscillator for ENSO. *J. Atmos. Sci.*, **45**, 3283-3287.

Vallis, G.K., 1988. Conceptual models of El Nino and the Southern Oscillation. *J. Geophys. Res.*, **93**, 13,979-13,991.

Yamagata, T., 1985: Stability of a simple air-sea coupled model in the tropics. In: *Coupled Ocean-Atmosphere Models*, J.C.J. Nihoul, ed., Elsevier: Amsterdam, 637-658.

Zebiak, S.E. and M.A. Cane, 1987: A model El Nino-Southern Oscillation. *Mon. Wea. Rev.*, **115**, 2262-2278.

WESTERN PACIFIC INTERNATIONAL MEETING AND WORKSHOP ON TOGA COARE

Nouméa, New Caledonia
May 24-30, 1989

PROCEEDINGS

edited by

Joël Picaut *
Roger Lukas **
Thierry Delcroix *

* ORSTOM, Nouméa, New Caledonia
** JIMAR, University of Hawaii, U.S.A.

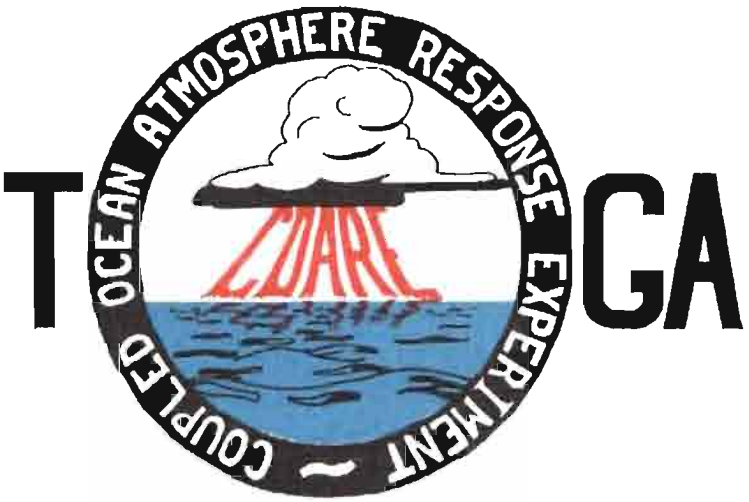

INSTITUT FRANÇAIS DE RECHERCHE SCIENTIFIQUE
POUR LE DÉVELOPPEMENT EN COOPÉRATION

ORSTOM

Centre de Nouméa

TABLE OF CONTENTS

MEETING COLLECTED PAPERS

WATER MASSES, SEA SURFACE TOPOGRAPHY, AND CIRCULATION

EL NINO/SOUTHERN OSCILLATION 1986-87

THEORETICAL AND MODELING STUDIES OF ENSO AND RELATED PROCESSES

MOMENTUM, HEAT, AND MOISTURE FLUXES BETWEEN ATMOSPHERE AND OCEAN

EMPIRICAL STUDIES OF ENSO AND SHORT-TERM CLIMATE VARIABILITY